

# Trapped-Particle Modes and Asymmetry-Induced Transport in Single-Species Plasmas

A. A. Kabantsev and C. F. Driscoll

*Physics Department, University of California, San Diego, California 92093-0319*

(Received 2 August 2002; published 25 November 2002)

A new asymmetry-induced transport mechanism in pure electron plasmas is shown to be proportional to the damping rate of the corresponding trapped-particle mode, with simple scalings for all other parameters. This transport occurs when axial particle trapping exists due to variations in the electric or magnetic confinement fields. This new transport is strong for even weak unintentional trapping ( $\delta B/B \sim 10^{-3}$ ), and may be prevalent in transport experiments with magnetic or electrostatic  $\theta$  asymmetries.

DOI: 10.1103/PhysRevLett.89.245001

PACS numbers: 52.27.Jt, 52.25.Fi, 52.35.-g

Single-species plasmas contained for long times in Penning-Malmberg traps are used for a wide range of experiments in plasma physics, atomic physics, beam physics, and fluid turbulence [1]. It is well known experimentally that  $\theta$  asymmetries in the magnetic or electric confinement fields cause plasma transport and loss to the walls [2–8], but quantitative comparison between experiments and theory [9] has been elusive.

In this Letter, a novel model of asymmetry-induced transport via dissipative trapped-particle modes [10–13] is characterized experimentally. The experiments are performed on quiescent pure electron plasma columns with enhanced axial particle trapping from a controlled  $\theta$ -symmetric “squeeze” voltage. This gives a well-defined trapped-particle mode, enabling accurate measurements of the mode damping rate  $\gamma_a$ .

The application of magnetic or electric “tilt” asymmetries to the trap then causes bulk radial plasma transport, as expected. The measured asymmetry-induced transport rates  $\nu_P$  have rather complicated dependencies on plasma temperature  $T$  and magnetic field  $B$ , but the data show that the complications are all associated with the mode damping rate  $\gamma_a$ . The scaled transport rate  $\nu_P/\gamma_a$  shows stunningly simple, accurate, and wide-ranging scalings for all plasma parameters.

The theory model motivated by these scalings is now being developed. Plasma rotation through the static  $m_\theta \neq 0$ ,  $k_z \neq 0$  field asymmetries necessarily generates dc equilibrium currents; similar tilt-induced *sloshing* currents have been previously identified [14], but not analyzed in depth. These currents couple nonresonantly to the trapped-particle mode with the corresponding  $m_\theta$  and  $k_z$  components. Velocity scattering across the trapped-particle separatrix causes mode damping, transforms electrostatic energy into kinetic energy, and produces bulk radial particle transport.

We believe that the asymmetry-induced transport observed in many axially long traps is dominated by this separatrix dissipation, *even when no trapping potentials are intentionally applied*. The trapping barriers can be either electric (as applied here) or small magnetic ripples.

On the present apparatus, the “anomalous” background transport is predominantly due to the 3% particle fraction trapped by magnetic ripples with  $\delta B/B = 10^{-3}$ .

Figure 1 shows the cylindrical confinement geometry of the “CamV” apparatus [15,16] and a schematic of the trapped-particle mode. The cylindrical column of electrons emitted from a hot tungsten source is confined radially by a “uniform” axial magnetic field  $1 \leq B \leq 10$  kG and confined axially by negative voltages  $-V_c = -100$  V on end cylinders of radius  $R_w = 3.5$  cm. The magnetic field can be aligned with the cylindrical electrode axis, or tilted at an angle  $0 \leq \alpha_B \leq 2 \times 10^{-3}$  rad to give an  $m_\theta = 1$ ,  $k_z = 1$  magnetic asymmetry. Electric asymmetries with  $m_\theta = 1$  or 2 give analogous results.

Typical electron columns have a central density  $0.5 \leq n_0 \leq 1.5 \times 10^7$  cm $^{-3}$  over a length  $38 \leq L_p \leq 49$  cm. The  $z$ -averaged densities  $n(r, \theta, t)$  are measured at any time by dumping the electrons axially onto a phosphor screen imaged by a CCD camera [15]. Varying the plasma radius over the range  $0.9 \leq R_p \leq 1.5$  cm varies the line density  $N_L \equiv \int r d\theta dr n(r, \theta, t)$ , with  $3 \leq N_L \leq 10 \times 10^7$  cm $^{-1}$ .

The electrons have adjustable thermal energy  $0.5 \leq T \leq 6$  eV, giving an axial bounce frequency  $f_b \equiv \bar{v}/2L_p \approx (0.5 \text{ MHz}) T^{1/2} (L_p/49)^{-1}$  and a Debye shielding length  $\lambda_D \approx (0.25 \text{ cm}) T^{1/2} (n/10^7)^{-1/2}$ . The electron space charge results in a central potential  $-\phi_p \approx (-30V)(N_L/6 \times 10^7)$ , and the radial electric field causes

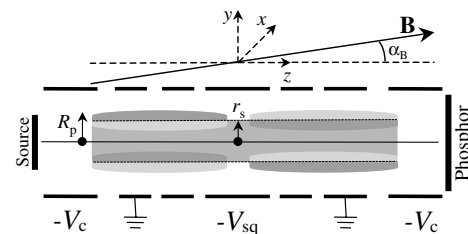


FIG. 1. Schematic of electron plasma with a trapped particle mode in the cylindrical containment system with adjustable magnetic tilt.

the column to  $\mathbf{E} \times \mathbf{B}$  drift rotate at a rate  $f_E(r) \equiv cE(r)/2\pi rB \approx (0.1 \text{ MHz})(n/10^7)B^{-1}$ . Thus, the plasma “rigidity”  $\mathcal{R} \equiv f_b/f_E$  is in the range  $1 \leq \mathcal{R} \leq 100$ .

We create trapped-particle populations by applying a negative  $\theta$ -symmetric squeeze voltage  $-V_{\text{sq}}$  to a short central cylinder. Electrons are excluded from the plasma periphery under the squeeze cylinder, and electrons with axial velocity less than the separatrix velocity  $v_s(r)$  are trapped axially in one end or the other. For small  $V_{\text{sq}}$ , a fraction

$$\frac{N_L^{\text{tr}}}{N_L} \approx 1.2 \left( \frac{V_{\text{sq}}}{\phi_p} \right) \quad (1)$$

of all the electrons are trapped, predominantly at radii  $r > r_s$ , defined by  $v_s(r_s) = \bar{v}$ .

The trapped-particle mode [12] of interest here is an  $m_\theta = 1$ , axially-antisymmetric drift mode propagating at frequency  $f_a$  on the otherwise  $\theta$ -symmetric column. The mode perturbations are essentially uniform on either side of the trapping barrier, but of opposite sign. The two trapped populations (at  $r > r_s$ ) execute oppositely-phased  $\mathbf{E} \times \mathbf{B}$  drift motions, analogous to two  $k_z = 0$ ,  $m_\theta = 1$  diocotron modes. Simultaneously, the untrapped particles (at  $r < r_s$ ) slosh from end to end and partially Debye shield the trapped perturbations. The mode frequency  $f_a$  is close to the rotation frequency  $f_E$  when  $V_{\text{sq}} \ll \phi_p$  gives weak edge trapping; and  $f_a$  becomes degenerate with the diocotron frequency  $f_d$  when  $V_{\text{sq}} \approx \phi_p$ .

This trapped-particle mode is relatively strongly damped [12], due to velocity-space diffusion of particles across the trapping separatrix. The damping rate  $\gamma_a$  depends strongly on  $T$  and  $B$ . Figure 2 shows the measured  $\gamma_a(T)$  together with a fit to the generic functional form  $A + B\exp(-C/T)$ . Recent experiments show that the damping depends on magnetic field as  $\gamma_a \propto B^{-0.5}$  for  $\mathcal{R} \gg 1$ , and as  $\gamma_a \propto B^{-1}$  for  $\mathcal{R} \leq O(1)$ ; this scaling was previously missed [12] because it was canceled by concurrent  $B$ -dependent temperature changes. The damp-

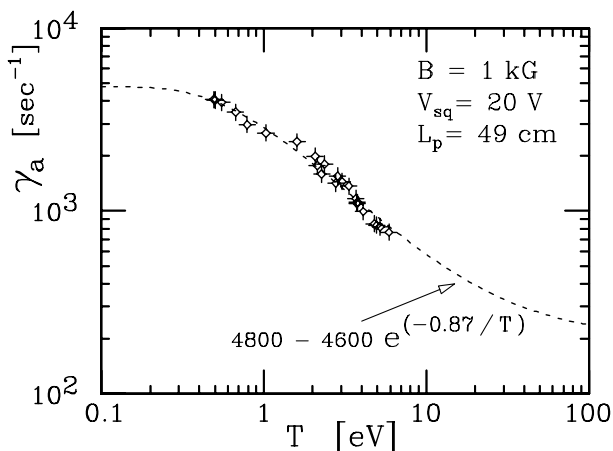


FIG. 2. Measured trapped particle mode damping rate  $\gamma_a$  versus plasma temperature  $T$ , with a generic exponential fit.

ing shows little dependence on  $N_L$  and  $L_p$  for  $\mathcal{R} \gtrsim 1$  and  $N_L^{\text{tr}}/N_L = \text{constant}$ .

Theory analysis of the damping requires a difficult boundary layer treatment, as originally developed for trapped-particle modes in neutral plasmas [10,11]. At present, theory estimates of  $\gamma_a$  for rigid plasmas [17] agree with measurements to within a factor of 2. The strong temperature dependence arises from the density of particles at the separatrix velocity  $v_s(r)$ ; at high temperatures the damping is determined by the trapped particles alone, and is expected to be independent of  $T$ .

If we now introduce  $\theta$  asymmetries in the electric or magnetic containment fields, the angular momentum of the plasma changes, and bulk radial expansion of the plasma occurs. Here we focus on the  $m_\theta = 1$ ,  $k_z = 1$  magnetic asymmetry induced by a magnetic tilt, with  $\mathbf{B} = B(\hat{z} + \alpha_B \hat{y})$ . The angular momentum is given by

$$P_\theta = (eB/c)N_{\text{tot}}[R_w^2 - \langle r^2 \rangle] + N_{\text{tot}}\langle mrv_\theta \rangle, \quad (2)$$

where  $\langle \rangle$  represents an average over all particles; here the kinetic momentum  $mrv_\theta$  is negligible. Thus, we characterize the asymmetry-induced transport rate by the rate of plasma expansion, as

$$\nu_P \equiv \frac{d}{dt} \langle r^2 \rangle / \langle r^2 \rangle \approx - \frac{d}{dt} P_\theta / P_\theta. \quad (3)$$

In practice, two measurements of  $n(r, \theta, t)$  separated in time by  $\Delta t = 0.1$  to 20 sec (chosen so that  $\delta \langle r^2 \rangle / \langle r^2 \rangle \leq 0.02$ ) give  $\nu_P$  with an accuracy of  $\pm 5\%$ .

The measured asymmetry-induced transport rates  $\nu_P$  show rather complicated dependencies on the plasma parameters of  $T$ ,  $N_L$ ,  $L_p$ , and  $B$ , but the transport rates are observed to be directly proportional to the mode damping rate  $\gamma_a$ . Figure 3 shows  $\nu_P \propto \gamma_a$  for a wide range of plasma parameters; the data set at 6 kG ( $\diamond$ ) was selected as illustrating the *worst* proportionality obtained.

For most data sets,  $\gamma_a$  was varied by increasing the overall plasma temperature  $T$  using standard rf heating [18,19]. For some data sets ( $\blacktriangledown$  in Fig. 3), a weak rf wiggle bounce resonant with the separatrix velocity further enhanced  $\gamma_a$  while giving negligible change in  $T$ . This separatrix control/diagnostic technique is exceedingly useful [13]; here it demonstrates unambiguously that the transport results from the same separatrix crossings as does the mode damping.

Data sets taken with controlled individual variations in  $B$ ,  $n$ ,  $R_p$ ,  $L_p$ ,  $T$ ,  $V_{\text{sq}}$ , and  $\alpha_B$  have now established the overall transport scaling to be

$$\frac{\nu_P}{\gamma_a} \approx 7.5 \times 10^{-5} \left( \frac{L_p}{R_w} \right)^2 \left( \frac{eN_L^2}{B} \right) \left( \frac{V_{\text{sq}}}{\phi_p} \right) \alpha_B^2. \quad (4)$$

Figure 4 displays all measured values of  $\nu_P/\gamma_a$ , with each point representing the slope of a data set (with symbols corresponding to Fig. 3). Figure 4 shows that the tilt-induced transport in trapped-population plasmas

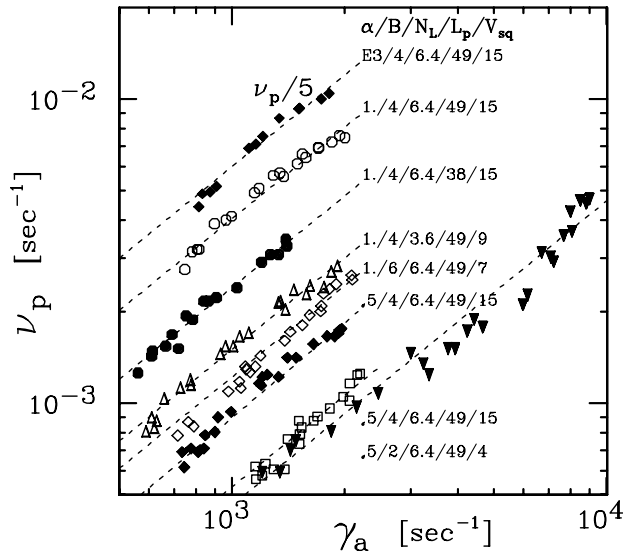


FIG. 3. Measured tilt-induced transport rate  $\nu_p$  versus the simultaneously measured mode damping rate  $\gamma_a$  for a variety of plasma, asymmetry, and trapping parameters.

is proportional to the trapped-particle mode damping rate over a parameter range of three decades in  $\nu_p/\gamma_a$ ; for perspective, the unscaled transport ranged over  $10^{-4} \leq \nu_p \leq 1 \text{ sec}^{-1}$ .

Similarly simple scalings are obtained for applied  $m_\theta = 1$  or 2 *electrostatic* asymmetries, alone or in combination with the magnetic tilt asymmetry. Figure 5 shows the transport induced by static  $m_\theta = 1$  asymmetry voltages  $V_{ax}$  or  $V_{ay}$  applied as  $\pm$  pairs to opposing sectors oriented in the  $\hat{x}$  or  $\hat{y}$  directions, in combination with the  $\alpha_B \hat{y}$  magnetic tilt. The transport scales as  $V_{ax}^2$  and as  $(V_{ay} - D)^2$ , similar to the  $\alpha_B^2$  scaling.

Indeed, the magnetic and electric tilt asymmetries can be put on an equal footing by considering the radial (off-

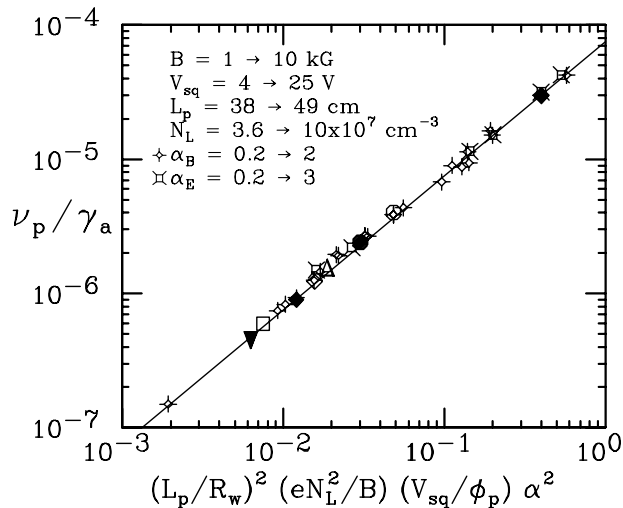


FIG. 4. Measured transport  $\nu_p$  normalized by mode damping  $\gamma_a$  versus scalings for all parameters.

axis) shift  $\Delta$  which the asymmetry induces. The magnetic tilt shifts each  $(L_p/2)$  half of the column off-axis by an average amount

$$\Delta_B = \frac{1}{2}\alpha_B(L_p/2). \quad (5)$$

The voltages  $\pm V_a$  applied to sectors of length  $L_a$  shift each half of the column off-axis by an amount

$$\Delta_E \approx 0.51R_w \left( \frac{V_a}{2eN_L} \right) \left( \frac{L_a}{L_p/2} \right) \equiv \alpha_E \left( \frac{L_p}{4} \right); \quad (6)$$

here the numerical coefficient represents the  $m_\theta = 1$  Fourier component of the applied voltage [16]. These center-of-mass shifts  $\Delta_E$  are measured by rapidly “cutting” the plasma axially, then dumping and measuring only the end of interest, to characterize the electric asymmetries of Fig. 3 ( $E3$ ,  $\alpha_E = 3 \text{ mrad}$ ) and Fig. 4.

The experiments thus determine a rather complete scaling law for tilt-asymmetry-induced transport in a long column with a *central* trapping barrier, as

$$\nu_p \approx 6.3 \times 10^{-5} \gamma_a \left( \frac{N_L^{\text{tr}}}{N_L} \right) \left( \frac{eN_L^2}{B} \right) \left( \frac{L_p}{R_w} \right)^2 [\underline{\alpha}_B + \underline{\alpha}_E]^2. \quad (7)$$

Here  $\underline{\alpha} = \alpha_x \hat{x} + \alpha_y \hat{y}$ , and we have used Eq. (1) for  $N_{\text{tr}}$ .

The applied electric and magnetic asymmetries can partially cancel each other, and temperature variations eventually cause deviations from  $V_a^2$  (Fig. 5, dashed vs dotted), leaving an illusory  $V_a^1$  dependence possibly seen in prior experiments [6,8]. We note that the  $\underline{\alpha}_B \cdot \underline{\alpha}_E$  cross term is only approximate, since the electric perturbation is applied at discrete  $z$  positions, so  $\Delta_E(z) \neq z \cdot \alpha_E$ ; the “overlap integral” between electric and magnetic tilts will generally be less than unity ( $\approx 0.8$  here).

Surprisingly, even weak *magnetic* barriers can dominate the asymmetry-induced transport. The dominant unintentional trapping on the CamV apparatus is due to magnetic ripples of magnitude  $\delta B/B \sim 10^{-3}$ , as shown in Fig. 6. These local magnetic mirrors give  $N_L^{\text{tr}}/N_L =$

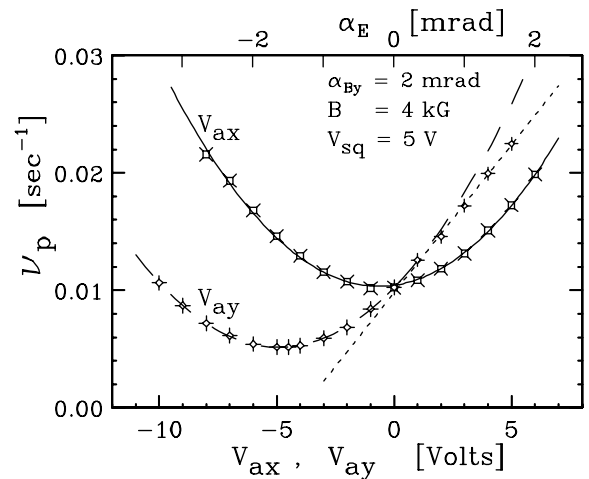


FIG. 5. Measured transport  $\nu_p$  from magnetic tilt and simultaneously applied *electric* asymmetry  $V_{ax}$  or  $V_{ay}$ .

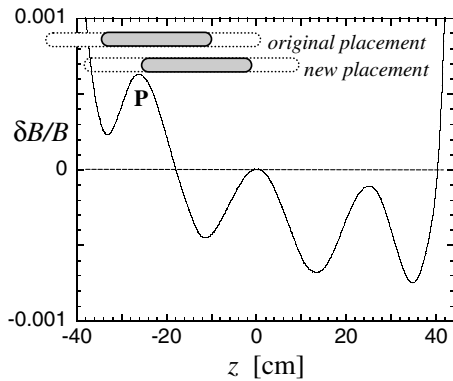


FIG. 6. Modified electrode placement relative to (vendor-measured) magnetic field  $B(z)$  exhibits  $5\times$  less background transport in the grey containment region.

$(\delta B/B)^{1/2} \approx 0.03$ . The original magnet position resulted in a peak (P) near the middle of the full containment region (dotted) and a 26 cm region (grey). Moving the magnet by  $\Delta z = 9$  cm placed the peaks at the ends of the 26 cm region, and resulted in a  $5\times$  decrease in the background transport for plasmas contained in this region.

This identification of magnetic trapping is further verified by techniques which *enhance* or *decrease* the separatrix diffusion. Application of bounce-resonant rf causes enhanced transport, and quantitatively diagnoses the particle density along the magnetic separatrix [13]. These separatrix resonances can also be driven by the plasma rotation through external asymmetries, possibly explaining resonances observed in multipolar magnetic mirrors [20]. Alternately, applying a small electric squeeze ( $V_{sq} \lesssim T/e$ ) in the magnetic mirror region decreases  $\nu_P$  (by up to  $5\times$ ) by excluding electrons from the magnetic separatrix.

The asymmetry-induced transport from magnetic trapping shows similar scalings with  $T$ ,  $L_p$ ,  $B$ ,  $\alpha_B$ , and  $\alpha_E$  (and is similar in magnitude) to that of Eq. (7). Differences will arise in that the parallel separatrix velocity  $v_s$  depends on  $v_\perp$  for magnetic trapping, and it is generally not a strong function of radius.

The transport scalings of Eq. (7) show strong correspondences to prior experiments. For magnetic field, we expect  $\nu_P \propto \gamma_a(B)B^{-1} \propto (B^{-1.5} \text{ to } B^{-2})$ , where the final range presumes the  $\gamma_a(B)$  scaling discussed above. The deviation from  $B^{-2}$  may have also been seen in prior experiments [7].

For length dependence, we observe  $\nu_P \propto L_p^2$  for fixed magnetic tilt  $\alpha_B$  (open and solid circles in Fig. 3), but expect (and have observed)  $\nu_P \propto L_p^{-2}$  for electric asymmetries, since fixed  $V_a$  and  $L_a$  give  $\alpha_E \propto L_p^{-2}$  in Eq. (6). The oft-observed (but approximate)  $L^2/B^2$  scaling [3] probably represents magnetic asymmetries acting on magnetically trapped populations; but other length scalings have also been observed [4,6], and Eq. (7) will not directly apply for noncentered (or multiple) trapping barriers.

For density dependence, Eq. (7) gives  $\nu_P \propto N_L^2$  for fixed magnetic tilts and fixed trapped-particle fraction; but can even give  $\nu_P \propto N_L^{-1}$  for fixed  $V_{sq}$  and fixed  $V_a$ . This is in general accord with the  $\nu_P \propto (n^{-1} \text{ to } n^2)$  dependence commonly observed [4–6,21], and adds a radius  $R_p$  dependence which has not been systematically studied experimentally.

The temperature dependence of  $\nu_P$  arises solely through the mode damping rate  $\gamma_a(T)$ , which shows exponential decreases in regions of experimental interest. This probably explains the abrupt decrease [6] in transport observed for rigidity  $\mathcal{R} \gtrsim 10$ . More importantly,  $\mathcal{R}$  is not a globally relevant scaling parameter for trapped-particle-mediated transport, since unperturbed particle parameters ( $f_b, f_E$ ) can not describe the nonlinearities of trapped orbits and non-Maxwellian separatrix velocity distributions.

We thank J. Yu for laboratory contributions, and T. Hilsabeck and T. O’Neil for continuing theory discussions. This work is supported by ONR Grant No. N00014-96-1-0239 and NSF Grant No. PHY-9876999.

- 
- [1] *Non-Neutral Plasma Physics IV*, edited by F. Andereg, AIP Conf. Proc. No. 606 (AIP, New York, 2002).
  - [2] J. H. Malmberg and C. F. Driscoll, Phys. Rev. Lett. **44**, 654 (1980).
  - [3] C. F. Driscoll *et al.*, Phys. Fluids **29**, 2015 (1986).
  - [4] J. Notte and J. Fajans, Phys. Plasmas **1**, 1123 (1994).
  - [5] B. P. Cluggish, Ph.D. thesis, University of California, San Diego, 1995.
  - [6] J. M. Kriesel and C. F. Driscoll, Phys. Rev. Lett. **85**, 2510 (2000).
  - [7] E. H. Chao, R. C. Davidson, S. F. Paul, and K. A. Morrison, Phys. Plasmas **7**, 831 (2000).
  - [8] D. L. Eggleston and B. Carrillo, in Ref. [1], pp. 369–377.
  - [9] D. L. Eggleston and T. M. O’Neil, Phys. Plasmas **6**, 2699 (1999).
  - [10] B. B. Kadomtsev and O. P. Pogutse, Sov. Phys. JETP **24**, 1172 (1967).
  - [11] M. N. Rosenbluth, D. W. Ross, and D. P. Kostomarov, Nucl. Fusion **12**, 3 (1972).
  - [12] A. A. Kabantsev *et al.*, Phys. Rev. Lett. **87**, 225002 (2001).
  - [13] A. A. Kabantsev and C. F. Driscoll, Rev. Sci. Instrum. (to be published).
  - [14] G. W. Hart, Phys. Fluids B **3**, 2987 (1991).
  - [15] K. S. Fine, W. G. Flynn, A. C. Cass, and C. F. Driscoll, Phys. Rev. Lett. **75**, 3277 (1995).
  - [16] J. M. Kriesel, Ph.D. thesis, University of California, San Diego, 1999.
  - [17] T. J. Hilsabeck and T. M. O’Neil, Bull. Am. Phys. Soc. **47**, 125 (2002).
  - [18] B. R. Beck, J. Fajans, and J. H. Malmberg, Phys. Rev. Lett. **68**, 317 (1992).
  - [19] B. P. Cluggish, J. R. Danielson, and C. F. Driscoll, Phys. Rev. Lett. **81**, 353 (1998).
  - [20] E. P. Gilson and J. Fajans, in Ref. [1], pp. 378–387.
  - [21] E. Sarid, E. Gilson, and J. Fajans, Phys. Rev. Lett. **89**, 105002 (2002).